Coverage-dependent formic acid oxidation reaction kinetics determined by oscillating potentials

Max J. Hülsey[1,#], Chia Wei Lim[1,#], Sie Shing Wong[1,2], and Ning Yan[1*]

[1] National University of Singapore, Department of Chemical and Biomolecular Engineering, 4 Engineering Drive 4, 117585 Singapore.

[2] Joint School of National University of Singapore and Tianjin University, International Campus of Tianjin University, Binhai New City, Fuzhou 350207, China.

[#] Authors contributed equally.

* Corresponding author: ning.yan@nus.edu.sg

Abstract

Establishing correlations between catalytic activity and dynamic surface properties of real catalysts, such as adsorbate coverage, is not straight-forward but crucial for the understanding of catalytic phenomena. The formic acid oxidation reaction comprises the non-Faradaic dehydration to CO when no potential is applied to the catalyst surface and the subsequent Faradaic oxidative desorption to form CO_2. Here, we report a methodology based on applying oscillating potentials to various electrocatalytically active metal surfaces during the formic acid oxidation reaction. Moderate frequency oscillations (0.1 to 10 Hz) allow us to control the coverage of intermediates on the surface, thus enable quantifying the transient effects (on the time scale of up to 10^{-4} s) of coverage on the reaction rate. We determined different coverage-dependences of turnover frequencies for Pt metal plate and various carbon-supported metal nanoparticle catalysts (Pt/C, Pd/C and Rh/C). This method therefore constitutes a valuable and simple tool for the elucidation of adsorbate coverages on metal surfaces and their resulting catalytic performance. We also demonstrate that dynamic catalytic processes can be analyzed semi-quantitatively with this new approach allowing the design of catalytic processes under optimized conditions.

1. Introduction

Dynamic effects of electric potentials on catalytic surfaces have been vastly ignored so far despite the wide-spread use of electroanalytic techniques like electrochemical impedance spectroscopy which relies on high-frequency potential changes. One of the earliest reports by Adžić *et al*. showed formic acid (FA) electrooxidation enhancements when 'pulsated potentials' with an amplitude of 600 mV and an ideal frequency of 2000 Hz were applied to a Pt electrode. Current density improvements on the order of 10^2 were achieved.[1] Similar trends were established for the methanol oxidation reaction on Pt surfaces again with current density increases of around 10^2.[2] Catalyst morphology changes under oscillating potentials were predicted by Kim *et al*.[3] who proposed that this may explain experimental catalytic results obtained earlier on Pd/$LiNbO_3$ catalysts.[4] Kakekhani *et al*. conducted systematic first-principle calculations on the effect of electric polarization switches for the reaction of NO and CO over RuO_2/$PbTiO_3$ and CrO_2/$PbTiO_3$. In line with previous simulations, they found that polarization could change the oxidation state of surface metals by up to ±1. Thus, depending on the polarization of the substrate, binding energies of adsorbates could be modified to different extents thus affecting surface coverages and reactivities. In this 'cyclic catalysis' manner, the authors proposed that the well-known Sabatier limit could be overcome.[5] In fact, the variation of adsorption energies by applied potentials and thus impacted catalytic performance has been investigated experimentally and theoretically before.[6-7] For oscillating potentials, enhancement effects have also been reported for the electrochemical adiponitrile synthesis.[8] Conventionally, the adiponitrile electrosynthesis suffers from undesired side reactions due to the concomitant accumulation of product and drop in substrate concentration in proximity to the electrode surface. Switching the surface polarization between two states with a square waveform enabled the fast reaction of substrate (cathodic time) as well as the diffusion of product from and substrate towards the electrode (anodic resting time). Beyond this, Blanco *et al*. claimed that electrolyte cations could diffuse towards the electrode during the anodic resting time,

which was reported to enhance the adiponitrile selectivity. Machine-learning aided optimization of various reaction parameters enabled improvements in the adiponitrile production rates and selectivities of 30% and 325%, respectively.[8] Based on insightful microkinetic modeling on the effects of dynamic switching of surface properties, Ardagh *et al*. revealed that both the reactivity as well as the selectivity of competing reactions can be modified dramatically if the changes in (relative) adsorption energies are sufficiently high. It was further predicted that oscillations need to be in approximate resonance with the surface reactions to achieve reaction enhancements.[9-12] DFT calculations by Shetty *et al.* revealed electric field-dependent linear scaling relationships of adsorbates on metal surfaces imperative for the understanding of dynamic catalytic processes.[13] Cycling between a potential suitable for the non-Faradaic dehydration of FA to surface-adsorbed CO and the Faradaic oxidative desorption to form CO_2 enhanced the activity by a factor of up to around 20 at frequencies of 100 Hz,[14] consistent with promotional effect observed by Adžić *et al*. earlier.[1]

Besides enhancing surface reactions, we envisage that oscillating potentials are capable of aiding the investigation of transient surface properties during catalysis. Transient effects are known to impact electrocatalytic reaction rates tremendously. One of those effects is the coverage of the surface with adsorbates affecting catalysis in diverse ways. For many multimolecular surface reactions, balanced relative adsorption strengths of all reactants are required for efficient surface reactions. Furthermore, lateral interactions between adsorbates as well as electronic effects that adsorbates have on metal atoms in close proximity play pivotal roles. Unfortunately, tools to study coverages and rates simultaneously on real catalysts in liquid phase reactions are rare and suffer from serious shortcomings. Some techniques (e.g., X-ray photoelectron spectroscopy and *in situ* electron microscopy) are not applicable to study reactions in solvents, while some others provide information on bulk solid materials (e.g., X-ray absorption spectroscopy, Mößbauer spectroscopy, X-way diffraction) thus offering limited insights into the surface chemistry. One of the most developed techniques to analyze surface chemistry during electrocatalysis is vibrational spectroscopy (IR/Raman) but the time resolution is often not sufficient to capture transient surface effects and it is not selective to electrocatalytic reactions.[15] Surface coverage with intermediates can also be influenced by poisoning the electrocatalytically active surface area with more inert metals although conclusions are also affected by bimetallic alloying effects.[16-17] Due to the inability of experimental approaches to investigate lateral adsorbate interactions, most available information stems from DFT calculations. For example, atomistic simulations reveal that, for the CO oxidation reaction, adsorbate-adsorbate interactions do not affect which metal is the most catalytically active but are capable of asymmetrically broadening volcano curves. This has been shown to be dependent on the type of the metal but those trends are not easily confirmed experimentally.[18]

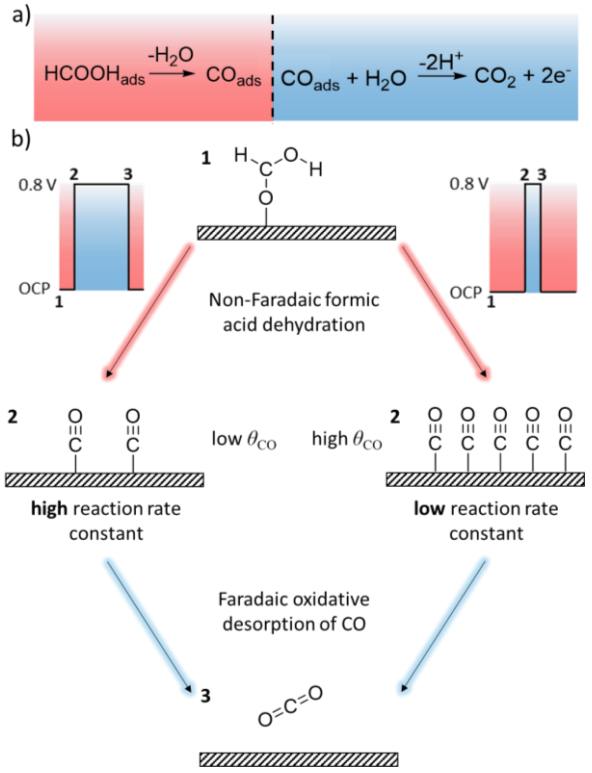

Figure 1. Overview of our electrochemical approach based on oscillating potentials. a) Non-Faradaic and Faradaic steps of the FA oxidation reaction; b) schematic of our approach for determining the coverage-dependent reaction rate constant.

Herein, we describe the development of a simple technique relying on the application of oscillating potentials between the open-circuit potential (OCP) and 0.8 V_{NHE} (potential against the normal hydrogen electrode) on different catalyst surfaces during the formic acid (FA) oxidation reaction. As reported previously, the open-circuit potential favors the non-Faradaic FA dehydration resulting in a metal surface covered with CO (**Figure 1a**). The oxidative desorption of CO only proceeds at higher potentials with the onset

around 0.8 V_{NHE}. Therefore, cycling between those two potentials enables controlled coverage of the surface with CO adsorbates (illustrated in red in **Figure 1b**) and the measurement of Faradaic reaction rate by detecting the current density (illustrated in blue in **Figure 1b**). We demonstrated that this approach allows us to determine CO coverage-dependent reaction rates on different metal surfaces.

2. Materials and Methods

2.1. Catalyst preparation and characterization

Carbon cloths (Xinke Experimental Materials Sales Center) were first pre-treated by immersing in 32.5% nitric acid, made from nitric acid (VWR Chemicals, 65%) and ultra-pure water (Milli-Q®), and heating at 80 °C for 24 h. The carbon cloths were then thoroughly rinsed with ultra-pure water and dried overnight. To prepare Pt/C catalyst ink, 2.1 mg of 5 wt% Pt/C (Sigma-Aldrich), 0.5 mg of Nafion® perfluorinated resin solution (Sigma-Aldrich, 5 wt% in 45% water balanced with lower aliphatic alcohols), 0.6 mg of finely ground activated charcoal (Sigma-Aldrich, 12-20 mesh granular DARCO®) and 700 µL of absolute ethanol (VWR chemicals, >99.7%) were mixed and sonicated for 1.5 h. For Pd/C catalyst ink, 1.1 mg of 10 wt% Pd/C (Sigma-Aldrich) and 1.6 mg of activated charcoal were used, while for Rh/C catalyst ink, 2.1 mg of 5 wt% Rh/C (Shaanxi Kaida Chemical Engineering Co. Ltd.) and 0.6 mg of activated charcoal were used. The prepared catalyst ink was transferred to both sides of a 1 × 1 cm pre-treated carbon cloth. The impregnated carbon cloths were dried at 80°C overnight and were then rinsed with and stored in ultra-pure water until use.

The JEM 2100F (JEOL, Japan) microscope was operated at 200 kV to collect transmission electron microscopy (TEM) images. A Bruker D8 Advance X-ray diffractometer was used to collect X-ray diffraction pattern of different commercial carbon-supported catalyst materials between 5 and 80°. The dispersion of the Pt plate electrode was estimated based on simple geometric arguments and the density of atoms per surface area for flat Pt surfaces (10^{19} m^{-2}). The dispersion of carbon-based catalysts was approximated based on the following empirical correlation which was shown to be valid for dispersions between around 20 and 92%:

$$D = \sqrt[1.23]{3.32 \times \frac{d_{\mathrm{at}}}{d_{\mathrm{AV}}}} \quad (1)$$

With D as dispersion, d_{at} as the atomic radius (200 pm for Rh, 163 pm for Pd, and 175 pm for Pt) and d_{AV} for the average particle size.[19]

2.2. Electrochemical setup and experiments

For all the experiments, a 200 cm^3 three-electrode electrochemical cell was used, with a Pt plate electrode (Shanghai Jingchong Electronic Technology Development Pte. Ltd.) as the counter electrode and a saturated calomel electrode (Shanghai Jingchong Electronic Technology Development Pte. Ltd.) as the reference electrode. The working electrode was either a Pt plate electrode or one of the impregnated carbon cloths prepared earlier. 150 cm^3 aqueous solution of 0.25 M FA (Sigma-Aldrich, >95%) and 0.25 M sulfuric acid (Sigma-Aldrich, 99.999%) was used as the electrolyte. Purified nitrogen gas (Air Liquide, 99.9995%) was continuously passed through the electrochemical cell at a rate of 35 mL min^{-1} starting from 1 h before experiments. The electrolyte solution was stirred at a constant speed of 800 rpm and all experiments were conducted at room temperature.

A Gamry Reference 3000 Potentiostat was used for all electrochemical measurements. To obtain the open circuit potential (OCP) of the electrochemical system, the measurement was conducted until the OCP reading stabilized within a tolerance of 10 mV for 500 s (**Figure S1**). For Cyclic Voltammetry (CV) measurements, a scan rate of 50 mV s^{-1} and a step size of 5 mV were used for Pt plate while a scan rate of 10 mV s^{-1} and a step size of 5 mV were used for the carbon-supported metal catalysts due to the very high current observed at higher scan rates. CV measurements were repeated until there was no further change between successive CV curves. For Electrochemical Impedance Spectroscopy (EIS) measurements, the frequency ranged from 1000 to 0.1 Hz with an AC voltage of 10 mV rms. Using the Gamry Virtual Front Panel software, oscillating electric potentials of square waveforms were applied to the working electrode at a data acquisition frequency of 5000 Hz. The maximum of the square waves was 0.8 V_{NHE} while the minimum was the OCP value measured earlier. The wave frequency ranged from 0.1 to 10 Hz while the duty cycle was varied between 0.01 and 99.995%. Each experiment involving oscillating potentials lasted 100 s and the data for last complete cycle was extracted for analysis. In this paper, all potential values have been reported with reference to the normal hydrogen electrode (NHE). CO_2 was separated and quantified with an Agilent 7890B gas

chromatograph with a TCD detector. At each static or dynamic potential, gas samples were taken continuously until three subsequent measurements showed deviations in CO_2 formation rates of below 1%. Calibrations were done with a 1% CO_2 (Air Liquide, balance N_2) gas mixture. Frequency (f) and duty cycle are defined as follows:

$$f = \frac{1}{t_{OCP}+t_{0.8V}} \quad (2)$$

$$\text{duty cycle} = \frac{t_{0.8V}}{t_{OCP}+t_{0.8V}} \times 100\% \quad (3)$$

3. Results and Discussion

3.1. Catalyst characterization

Pt plate electrodes were purchased and used as received while commercial Pt/Pd/Rh nanoparticles supported on carbon were prepared by drop-casting their ethanol-based inks on carbon cloth. TEM images were used to determine the average particle size for the commercial carbon-based catalysts. 1.95 ± 0.34 nm, 2.82 ± 0.41 nm, and 5.4 ± 0.95 nm were identified for Pt, Pd, and Rh/C, respectively (**Figure S2**). XRD patterns for each of the materials show no clear diffraction peaks for these metals confirming the size of metal particles to be small (**Figure S3**). Using equation (1), dispersions were estimated to be 26% for Pd/C, 37% for Pt/C, and 18% for Rh/C. Those values are consistent with previous studies on comparable carbon-supported catalysts.[20] Therefore, we calculated the turnover frequencies on carbon-based catalysts based on the dispersion values while the number of sites of the Pt plate electrode was calculated based on the total surface area and the approximate Pt site density.

CV scans with sulfuric acid/FA electrolytes on Pt plate electrodes revealed two redox features during the anodic trace (**Figure 2**). The first one centered at around 0.5 V is commonly associated to Faradaic FA oxidation reactions to surface formate or hydroxy carbonyl intermediates while the second one occurs due to the Faradaic CO oxidative desorption reaction. For carbon-based electrodes, the CV peaks are less easily discernable but similar peak shapes to Pt plates have been reported before.[21-24]

The effect of oscillating potentials on the FA oxidation reaction on Pt plate electrodes has been investigated and we identified a frequency of 100 Hz at a duty cycle of 50% between OCP and 0.8 V to yield the largest FA oxidation enhancement (**Figure S4**) in accordance to a previous study.[14] In the following, we further elucidated the transient current responses upon potential switches and we explored the capability of oscillating potentials in illuminating reaction kinetics.

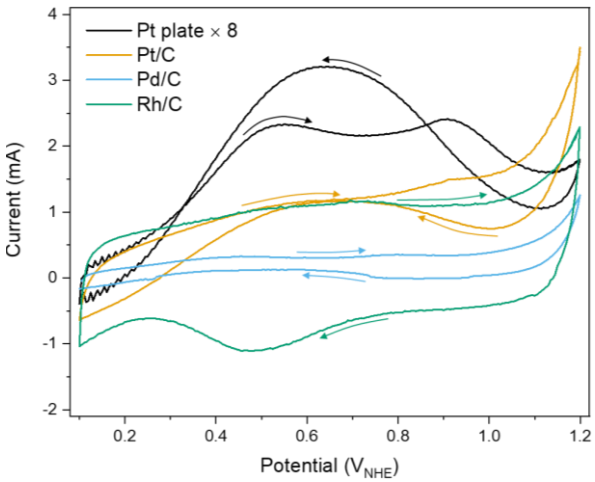

Figure 2. CV scans of different catalysts in 0.25 M H_2SO_4 and 0.25 M FA. Scan rates were 10 mV s^{-1} (for Pt plate: 50 mV s^{-1}).

3.2. Modelling of transient current responses

Applying oscillating potentials between the OCP and 0.8 V on electrodes in sulfuric acid/FA electrolyte gave transient current responses which should arise mostly due to the Faradaic oxidation of CO on the electrode surface. As shown in **Figure 3**, the current decays in an exponential-like manner over time.

At OCP, the dehydration of FA takes place and the produced CO is adsorbed on the metal catalyst surface. When the potential changes from OCP to 0.8 V, the adsorbed CO starts to undergo Faradaic oxidative desorption, resulting in a current flow. Simultaneously, the adsorption and dehydration of FA is severely prohibited at this high potential as shown earlier.[25] The turnover frequency (TOF) for oxidative desorption was modelled as:

$$\text{TOF} = k_1\theta \quad (4)$$

where k_1 is the reaction rate constant and θ represents CO coverage on the catalyst surface.

The current flow, $I_{reaction}$, due to oxidative desorption of CO was given by:

$$I_{reaction} = \text{TOF} \times N_{sites} \times m \times F \quad (5)$$

where N_{sites} is the number of moles of active sites on the catalyst surface, m (= 2) is the number of electrons given out for each CO oxidized and F (= 96500 C mol^{-1}) is the Faraday constant.

Since $\text{TOF} = -\frac{d\theta}{dt}$, integration of (4) gave

$$\theta = \theta_\text{i} \exp(-k_1 t) \quad (6)$$

where θ_i is the CO coverage at $t = 0$.

Combining (5) and (6), the current can be represented as:

$$I_\text{reaction} = N_\text{sites} \times m \times F \times k_1 \times \theta_\text{i} \exp(-k_1 t) \quad (7)$$

We found that the transient current response of our system cannot be modelled sufficiently well by a single exponential term, suggesting that the current response comprises a more complex physical behavior than initially assumed (*vide infra*). This led us to the assumption that the impedance response of electrochemical systems under rapidly oscillating potentials might be non-negligible. Any electrochemical system gives current responses whenever the applied potential is changed, even in the absence of any reaction, due to its inherent impedance. Electrochemical impedance spectra were fitted with the system modelled as a Randles circuit, which consists of two resistors (bulk electrolyte resistance, R_1 and charge transfer resistance, R_2) and a capacitor (interfacial double-layer capacitance, C). R_2 is in parallel with C, while both of them are in series with R_1 (**Figure S5**).[26-27] We used V_A and V_B to denote the potential differences across R_1 and the parallel branch of R_2 and C respectively. Letting I_A and I_B be the currents through R_2 and C respectively, the current response, $I_\text{background}(t)$, of a Randles circuit following a step increase in applied potential from open circuit to V at $t = 0$ was derived:

$$V_\text{A} = (I_\text{A} + I_\text{B}) R_1 \quad (8)$$

$$V_\text{B} = I_\text{A} R_2 = \frac{1}{C} \int I_\text{B} dt \quad (9)$$

$$V = V_\text{A} + V_\text{B} = (I_\text{A} + I_\text{B}) R_1 + I_\text{A} R_2$$
$$\Longrightarrow I_\text{A} = \frac{V - I_\text{B} R_1}{R_1 + R_2} \quad (10)$$

Alternatively, we can also write

$$V = V_\text{A} + V_\text{B} = (I_\text{A} + I_\text{B}) R_1 + \frac{1}{C} \int I_\text{B} dt \quad (11)$$

Differentiating (11) with respect to t,

$$\frac{dV}{dt} = \left(\frac{dI_\text{A}}{dt} + \frac{dI_\text{B}}{dt}\right) R_1 + \frac{1}{C} I_\text{B} \quad (12)$$

Since $\frac{dV}{dt} = 0$ when $t > 0$ for a step change, combining (10) and (12) gave

$$\left[\frac{1}{R_1 + R_2}\left(\frac{dV}{dt} - R_1 \frac{dI_\text{B}}{dt}\right) + \frac{dI_\text{B}}{dt}\right] R_1 + \frac{1}{C} I_\text{B} = 0 \quad (13)$$

Using again $\frac{dV}{dt} = 0$ and after some rearrangement,

$$\frac{dI_\text{B}}{dt} = -\frac{1}{C} \frac{R_1 + R_2}{R_1 R_2} I_\text{B} \quad (14)$$

Integration of (14) gave

$$I_\text{B} = I_\text{Bi} \exp\left(-\frac{1}{C} \frac{R_1 + R_2}{R_1 R_2} t\right) \quad (15)$$

where I_Bi is the current through the capacitor at $t = 0^+$.

Now, using (10),

$$I = I_\text{A} + I_\text{B}$$
$$= \frac{1}{R_1 + R_2}\left[V - R_1 I_\text{Bi} \exp\left(-\frac{1}{C} \frac{R_1 + R_2}{R_1 R_2} t\right)\right]$$
$$+ I_\text{Bi} \exp\left(-\frac{1}{C} \frac{R_1 + R_2}{R_1 R_2} t\right) \quad (16)$$

Simplifying gave

$$I_\text{background}(t)$$
$$= \frac{V}{R_1 + R_2} + \frac{R_2}{R_1 + R_2} I_\text{Bi} \exp\left(-\frac{1}{C} \frac{R_1 + R_2}{R_1 R_2} t\right) \quad (17)$$

The values of resistances and capacitance were obtained from fitting the EIS results in a dilute sulfuric acid electrolyte using the Randles circuit model (**Figure S5**): R_1 = 2.525 Ω, R_2 = 9.519 × 10^3 Ω, C = 7.06 × 10^{-4} F. Since R_2 was much greater than R_1, the expression for $I_\text{background}(t)$ can be simplified to give

$$I_\text{background}(t) = I_\text{Bi} \exp\left(-\frac{t}{R_1 C}\right) \quad (18)$$

Physically, this implies that the current I_A through resistor R_2 is much smaller compared to the current through the capacitor, I_B. This is because the resistance, R_2, was much larger in magnitude than the capacitor impedance, C. The electrochemical system effectively behaved like a simple RC series circuit with an exponentially decaying current response when subject to a step change in applied potential from an initial state of open circuit.

From above, the current measured during the high potential cycle (0.8 V) of the electrochemical experiments is the sum of the two contributions: (1)

current due to electron transfer for the oxidative desorption of CO, and (2) background current response due to impedance of the electrochemical system. The following equation was used to model the current measured, I_{total}, to obtain the relevant parameters through minimizing the residual sum of squares (RSS):

$$I_{\text{total}} = I_{\text{reaction}} + I_{\text{background}} = A_1 \exp(-k_1 t) + A_2 \exp(-k_2 t) \quad (19)$$

where $A_1 = N_{\text{sites}} \times m \times F \times k_1 \times \theta_i$, $A_2 = I_{\text{Bi}}$ and $k_2 = \frac{1}{R_1 C}$.

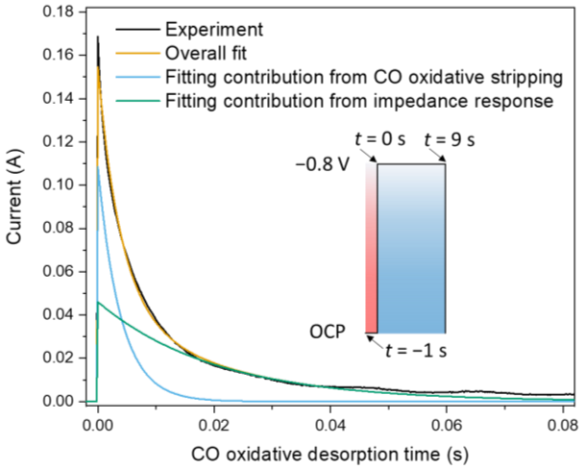

Figure 3. Transient current response during square wave shaped potential oscillations at 0.1 Hz (90% duty cycle). Different contributions to the experimentally observed current response were plotted alongside the overall fit. The plotted current response was directly after switching from OCP to 0.8 V. The inset explains the starting time of the current response curve.

Figure 3 shows the transient current response as the potential was switched from OCP to 0.8 V, using a 90%-duty square waveform oscillating at 0.1 Hz. The attempt to fit the measured current with a single-term exponential function was not satisfactory, confirming the need for a more complex model, such as the two-term model proposed above. The RSS-minimizing fitting procedure gave an optimized model that agreed well with the experimental data. The exponential term due to the oxidative desorption of CO contributed to majority of the initial current and decayed relatively quickly with time while the term due to the impedance of the electrochemical system started with a smaller initial value but decayed much more slowly. This general trend ($A_1 > A_2$ and $k_1 > k_2$) was seen in the optimized parameters obtained from fitting the transient current response under applied oscillating potentials of different frequencies and duty cycles (**Tables S1-S4**). The values of k_2 obtained did not vary significantly across different experimental conditions, which was characteristic of current response due to the electrochemical impedance. Furthermore, as shown in **Table S1**, the optimized values of k_2 matched well with the values of $R_1 = 2.873\ \Omega$, $C = 4.840 \times 10^{-3}$ F and $\frac{1}{R_1 C} \approx 71.9\ s^{-1}$ obtained from EIS measurements in a sulfuric acid/FA electrolyte.

Furthermore, the validity of our approach was confirmed by correlating the CO_2 formation rate (measured by gas chromatography) with the average rate of electron transfer, obtained by averaging the integrated current during dynamic catalytic reaction conditions over the oscillation period. A linear correlation was found between electron transfer and CO_2 productivity with a gradient of $1.7 \pm 0.1\ \text{mol}_e\text{-mol}_{CO_2}^{-1}$ in accordance with the theoretical number of electrons transferred for each molecule of CO oxidized (= 2) within experimental errors (**Figure S6a**). Good accordance between the number of transferred electrons and the CO_2 production rate was found for various static potentials as well (**Figure S6b**). Those results confirmed that our approach for determining the current due to Faradaic reactions was a viable and experimentally efficient method for quantifying the rate of FA oxidation to CO_2.

3.3. Evaluation of FA dehydration kinetics and CO coverage

Since the non-Faradaic FA dehydration reaction proceeded during the OCP part of the cycle, *the CO coverage could be increased by elongating t_{OCP} and vice versa*. With our just established protocol, CO coverage could be determined by integrating the current response due to the Faradaic CO oxidative desorption during the whole $t_{0.8V}$.

$$\int_0^{t_{0.8V}} A_1 \exp(-k_1 t) dt = \frac{A_1}{k_1}[1 - \exp(-k_1 t_{0.8V})] \quad (20)$$

For each experiment, $\int_0^{\infty} A_1 \exp(-k_1 t) dt$ was also evaluated and verified to be approximately equal (within 0.1% difference) to $\int_0^{t_{0.8V}} A_1 \exp(-k_1 t) dt$, ensuring that practically all CO had been desorbed from the catalyst surface before the next cycle began. As mentioned earlier, this approach is valid since at 0.8 V, the FA adsorption was reported to be negligible.[25] We

varied the FA dehydration time systematically (t_{OCP}) between 5 × 10^{-4} and 5 s. This was done both by adjusting the duty cycle as well as the frequency of the square waveform in order to avoid artifacts caused by either of those two parameters. For each metal catalyst, the value of $\int_0^{t_{0.8V}} A_1 \exp(-k_1 t)dt$ was plotted against the dehydration time. As shown in **Figure 4**, as the dehydration time increased, the surface coverage reached a maximum value, θ_{max}. Since differing reports exist on the exact surface fraction that can be covered by CO with θ_{max} values ranging from 0.5 to 0.8,[28-32] the coverage was simply represented as fraction of the maximum coverage, θ/θ_{max}, throughout the study:

$$\frac{\theta}{\theta_{\max}} = \frac{\int_0^{t_{0.8V}} A_1 \exp(-k_1 t)dt}{(\int_0^{t_{0.8V}} A_1 \exp(-k_1 t)dt)_{\max}} \quad (21)$$

Differences between electrodes were mainly assumed to be due to dispersion since the absolute coverages of all three metals are relatively similar. A particularly stark contrast was found for carbon-supported Pt and Pt plate electrodes which likely was due to the vast differences in surface areas.

Surprisingly, the times required to achieve $\theta_{max}/2$ were 0.19 s for Rh/C, 0.15 s for Pd/C, 0.007 s for Pt/C and 0.006 s for Pt plate. This indicated that the non-Faradaic FA dehydration reaction rates were vastly different for different metals by almost two orders of magnitude but appeared to be insensitive to the structure of the catalyst since Pt/C and the Pt plate electrode exhibited comparable dehydration rates. Since the FA dehydration kinetics follow the trend of Rh < Pd << Pt consistent with their observed reactivity, this finding alone appears to be sufficient to rationalize reactivity trends among the three noble metals.[33-35]

3.4. Coverage-dependent kinetics of CO oxidative desorption

After evaluation of the maximum coverage of CO on the different electrode surfaces, we determined the kinetics for the Faradaic CO oxidative desorption. k_1 and initial TOF (i.e. at the start of the high potential cycle) were plotted against θ/θ_{max}. A power law index, n, was used to quantify the variation of k_1 with θ/θ_{max}. As seen in **Figure 5a**, at full coverage, the reaction rate constants of Pd/C and Rh/C were comparable and around 100 s^{-1} while Pt/C had roughly three times higher rate constants. We noticed that reaction rate constants were significantly higher at fractional coverage providing a linear correlation between coverage and reaction rate constants in a double-log plot with the power law index n as the slope. Similar n values were determined for the three carbon-supported catalysts (−0.52, −0.58, and −0.53 for Pt/C, Pd/C, and Rh/C, respectively). Pt plate electrodes showed a significantly lower n value of −0.36 indicating the much lower sensitivity of reaction rates to coverage on polycrystalline Pt. It became apparent that the impact of surface CO coverage on the oxidative desorption activity is almost independent of the metals for nanoparticulate catalysts. However, the morphology of the surface appeared to influence the coverage-dependence.

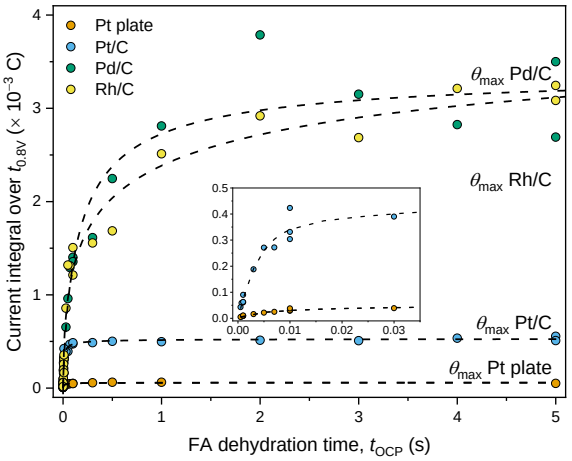

Figure 4. Dependence of integrated current for oxidative CO desorption on the FA dehydration time. The maximum coverage for each electrode is achieved at larger FA dehydration times. The inset shows the enlarged region for Pt/C and Pt plate electrodes.

We noted that the experimentally determined variation of reaction rate constant with coverage implied that the exponential model presented in (7) may not be entirely valid. Therefore, we have quantified the percentage differences between predictions by (7) and a model that allows for coverage-dependent rate constants and shown that they were always < 10% and thus negligibly small (details in and below **Figure S7**). Therefore, (7) was nevertheless appropriate for modelling the Faradaic part of the reaction, since most of the oxidative desorption happened in a short time, with a rate constant approximately equal to the value that corresponded to the initial coverage.

Similar trends can be observed in **Figure 5b** for the coverage-dependence of the initial turnover frequencies on the different electrodes. Since the TOFs are dependent on the absolute coverage of CO, there is a declining trend as lower relative coverages of CO are achieved. However, the highest reaction rate constants

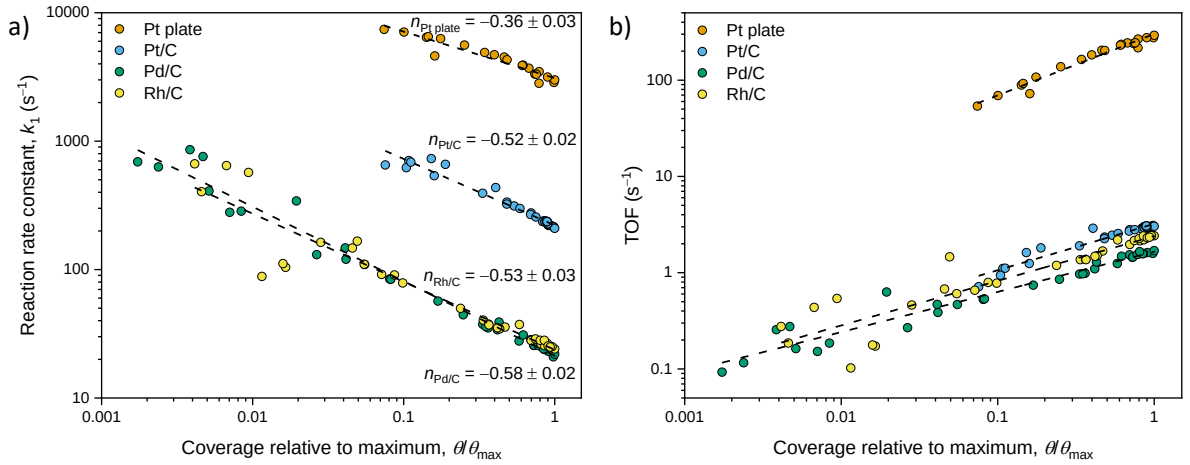

Figure 5. Dependences of reaction rate constant and initial turnover frequency of oxidative desorption of CO on relative surface coverage for different metal catalysts. Values of n for power law "$k_1 = a\theta^n$" are shown

are achieved at fractional coverage of the surface with CO. Differences in the CO oxidative desorption reaction rates are relatively minor compared to the relative rates for FA dehydration as mentioned earlier. This indicates that differences among the three carbon-supported noble metals are almost completely due to differences in the non-Faradaic reaction rates rather than the CO oxidative desorption. As far as we are aware, not many experimental approaches enable the quantitative kinetic analysis of individual reaction steps of electrocatalytic reactions.

Generally, the flatter Pt plate electrode surface seems to exhibit a much less pronounced coverage dependence and significantly higher reaction rates in comparison to the noble metal nanoparticles. This can in principle be rationalized by the interplay of three effects: a diversity of sites with varying adsorption energies as well as CO oxidation activities, lateral interactions between adsorbates at higher CO coverage, as well as different mechanisms dependent on θ_{CO} or the type of catalyst. Surface science studies showed that for Pt and Rh surfaces in acidic solutions at positive potentials, lower CO coverages favored the adsorption of CO in a bridged fashion. Since we observed that the CO oxidation reactivity is higher at lower coverage, we could ascribe the highest activity to bridged CO adsorption sites consistent with previous studies demonstrating that oxidation of bridged CO on terrace sites occurs at lower over-potentials compared to terminal sites.[36] This would also help rationalize the vastly enhanced TOF values for the flat Pt plate electrode which contains more terrace sites suitable for bridged CO adsorption in contrast to nanoparticles where the curvature favors linearly adsorbed CO. Since the CO oxidative desorption is believed to follow a Langmuir-Hinshelwood (LH) mechanism on most noble metal surfaces, the co-adsorption of water and CO is essential. Hence, excessive θ_{CO} values prevent the adsorption of co-reactant while the co-adsorption of water was also observed to favor the formation of bridged CO species further enhancing reactivity.[28, 37]

Although contributions of alternative mechanisms like the Eley-Rideal mechanism can be assumed to be negligible under our reaction conditions,[38] variations for the LH mechanism have been reported before. Island versus random oxidation mechanisms are commonly discussed, the former of which comprises the formation of adsorbed CO islands which tend to react on the rim while the latter indicates the reaction of a CO molecule homogeneously located on the electrode surface. Adsorbate islands are a common phenomenon for multimolecular reactions following an LH mechanism since lateral adsorbate interactions often favor spatial segregation of adsorbates. In the case of the CO oxidative desorption, lateral adsorbate–adsorbate interactions are so far rather poorly understood and different effects have been proposed depending on the electrode material.[39-40] Nonetheless, on the extended surface of the Pt plate electrode, such an island mechanism might indeed play a role and while excessively large islands due to high CO coverage limit the interfacial area between CO and water adsorbates, a negative CO reaction order could be easily rationalized.[41-43] Due to the small particle sizes of carbon-supported electrodes, CO islands cannot be assumed to exist. The fact that the Pt plate and nanoparticulate metal electrodes exhibit such distinct TOFs supports the hypothesis that the mechanisms are very different on those surfaces.

3.5. Optimize dynamic catalytic processes for formic acid oxidation

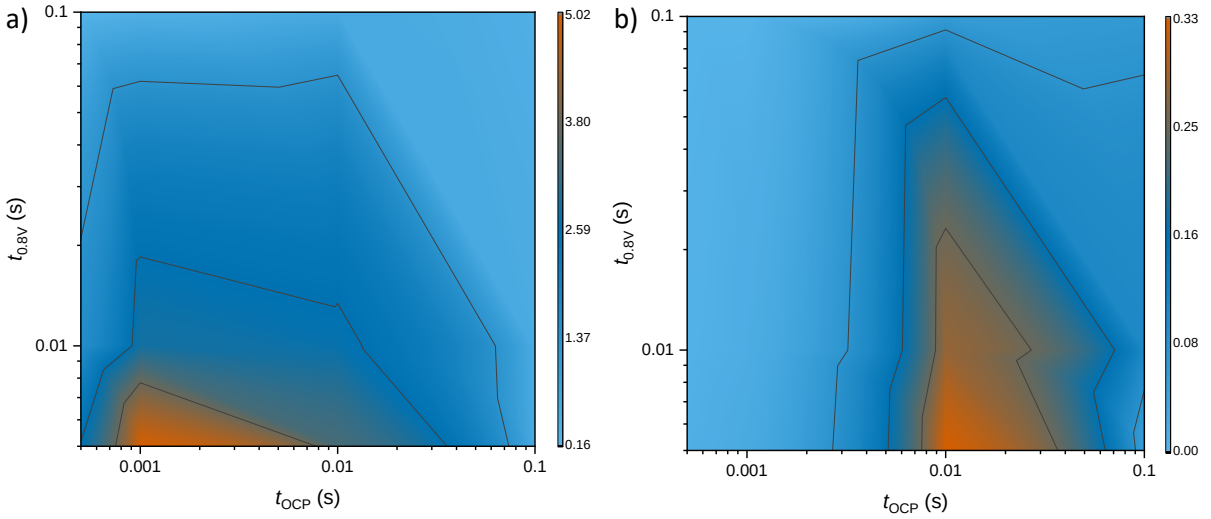

Figure 6. TOF dependence on t_{OCP} and $t_{0.8V}$ for a) Pt plate and b) Pd/C. Reactions were conducted with varying frequencies and duty cycles to match the values for t_{OCP} and $t_{0.8V}$. TOF values are given in s^{-1}.

In addition to providing fundamental insights into electrocatalytic reaction kinetics and coverage-dependent reaction rates, this tool also help with rationally designing dynamic catalytic processes. Based on the kinetic data, it is relatively straight-forward to assume that for different electrodes, dissimilar frequencies and duty cycles might lead to optimized activity. We thus went on to explore the 2-dimensional parameter space spanning both t_{OCP} and $t_{0.8V}$ for the Pd/C and Pt plate electrodes (**Figure 6**), in which TOFs were determined using the integrated current. For the Pt plate electrode, the activity optimum occurs at t_{OCP} = 0.001 s while $t_{0.8V}$ should be kept at or below 0.005 s. The ideal dynamic catalytic conditions can thus be achieved at approximately 170 Hz and a duty cycle of 80%, consistent with previous reports and our own CO_2 productivity data (**Figure S4**). This ideal t_{OCP} correlates to a CO coverage of around 50%. Since the time required to achieve a residual CO coverage of about 0.1% is $t_{0.8V} = \frac{1}{k_1} \times 6 = 0.002$ s < 0.005 s, conclusions drawn from **Figure 6a** might overestimate the ideal $t_{0.8V}$ slightly. For Pd/C (**Figure 6b**), ideal t_{OCP} and $t_{0.8V}$ are 0.01 s and smaller or equal to 0.005 s, respectively. This t_{OCP} optimum is consistent with an ideal initial CO coverage of roughly 10% which can be explained by the relatively high susceptibility of the CO oxidation activity to coverage compared to the Pt plate electrode. The optimum frequency and duty can be assumed to be around 70 Hz and a duty cycle around 30%. A more distinct optimum (t_{OCP} = 0.01 s, $t_{0.8V}$ = 0.01 s) was found when the FA oxidation reaction was carried out at 270 K under otherwise identical reaction conditions (**Figure S8**) with results largely consistent with the reaction at room temperature. This again illustrates that a compromise has been reached between a surface with sufficient fractional coverage without lowering the reaction rate significantly. Electrodes with a larger coverage dependence on the reaction rate exhibit optima at significantly lower coverages, which is usually difficult to accomplish without oscillating potentials. In general, it appears that for reactions with kinetically connected steps as is the case for FA oxidation, correlations between the activity and frequency are not straight-forward and thus kinetics for individual steps must be considered for the design of dynamic catalytic processes.

4. Conclusions

In conclusion, we have demonstrated the use of oscillating potentials for the analysis of FA oxidation kinetics. We found that electrodes based on different metals exhibit very different reaction kinetics for the non-Faradaic FA dehydration and the oxidative desorption of CO rationalizing the performance difference between Rh, Pd and Pt. Surprisingly, the main contribution to catalytic activity differences appears to arise from the FA dehydration reaction. Furthermore, we determined coverage-dependent reaction rate constants during the CO oxidative desorption, with particularly big differences between nanoparticulate and polycrystalline Pt observed. Although coverage-dependencies of electrocatalytic reactions (e.g. HER, ORR) have been observed and simulated before, we offer one of the first quantitative experimental elucidations.[44-46] Those results also helped us rationalize and optimize dynamic catalytic processes for formic acid oxidation. We envisage that those insights will be useful to guide the design of dynamic catalytic processes in the future, since the presented approach works in principle for any reaction

that involves separate non-Faradaic and Faradaic reaction steps.

Acknowledgements

This research is supported by the NUS Flagship Green Energy Program (R-279-000-553-646, and R-279-000-553-731). M. J. H. thanks the SINGA scholarship for supporting his PhD studies.

References

1. Adžić, R. R.; Popov, K. I.; Pamić, M. A., Acceleration of electrocatalytic reactions by pulsation of potential: Oxidation of formic acid on Pt and Pt/Pb_{ads} electrodes. *Electrochim. Acta* **1978,** *23* (11), 1191-1196.
2. Fedkiw, P. S.; Traynelis, C. L.; Wang, S. R., Pulsed - Potential Oxidation of Methanol. *J. Electrochem. Soc.* **1988,** *135* (10), 2459-2465.
3. Kim, S.; Schoenberg, M. R.; Rappe, A. M., Polarization Dependence of Palladium Deposition on Ferroelectric Lithium Niobate (0001) Surfaces. *Phys. Rev. Lett.* **2011,** *107* (7), 076102.
4. Inoue, Y.; Yoshioka, I.; Sato, K., Polarization effects upon adsorptive and catalytic properties. 1. Carbon monoxide oxidation over palladium deposited on lithium niobate ($LiNbO_3$) ferroelectrics. *J. Phys. Chem.* **1984,** *88* (6), 1148-1151.
5. Kakekhani, A.; Ismail-Beigi, S., Ferroelectric-Based Catalysis: Switchable Surface Chemistry. *ACS Catal.* **2015,** *5* (8), 4537-4545.
6. Neophytides, S. G.; Tsiplakides, D.; Stonehart, P.; Jaksic, M. M.; Vayenas, C. G., Electrochemical enhancement of a catalytic reaction in aqueous solution. *Nature* **1994,** *370* (6484), 45-47.
7. Hülsey, M. J.; Lim, C. W.; Yan, N., Promoting heterogeneous catalysis beyond catalyst design. *Chem. Sci.* **2020,** *11* (6), 1456-1468.
8. Blanco, D. E.; Lee, B.; Modestino, M. A., Optimizing organic electrosynthesis through controlled voltage dosing and artificial intelligence. *Proc. Natl. Acad. Sci. U.S.A.* **2019,** *116* (36), 17683-17689.
9. Ardagh, M. A.; Abdelrahman, O. A.; Dauenhauer, P. J., Principles of Dynamic Heterogeneous Catalysis: Surface Resonance and Turnover Frequency Response. *ACS Catal.* **2019,** *9* (8), 6929-6937.
10. Ardagh, M. A.; Birol, T.; Zhang, Q.; Abdelrahman, O. A.; Dauenhauer, P. J., Catalytic resonance theory: superVolcanoes, catalytic molecular pumps, and oscillatory steady state. *Catal. Sci. Technol.* **2019,** *9* (18), 5058-5076.
11. Ardagh, M. A.; Shetty, M.; Kuznetsov, A.; Zhang, Q.; Christopher, P.; Vlachos, D. G.; Abdelrahman, O. A.; Dauenhauer, P. J., Catalytic resonance theory: parallel reaction pathway control. *Chem. Sci.* **2020,** *11* (13), 3501-3510.
12. Shetty, M.; Walton, A.; Gathmann, S.; Ardagh, M. A.; Gopeesingh, J.; Resasco, J.; Birol, T.; Zhang, Q.; Tsapatsis, M.; Vlachos, D. G.; Christopher, P.; Frisbie, C. D.; Abdelrahman, O. A.; Dauenhauer, P. J., The Catalytic Mechanics of Dynamic Surfaces: Stimulating Methods for Promoting Catalytic Resonance. *ACS Catal.*, in press.
13. Manish, S.; Matthew, A.; Yutong, P.; Omar, A.; Paul, D., Electric-Field Assisted Modulation of Surface Thermochemistry. *ChemRxiv* **2020,** https://doi.org/10.26434/chemrxiv.12127191.v1.
14. Gopeesingh, J.; Ardagh, M. A.; Shetty, M.; Burke, S. T.; Dauenhauer, P. J.; Abdelrahman, O. A., Resonance-Promoted Formic Acid Oxidation via Dynamic Electrocatalytic Modulation. *ACS Catal.* **2020,** *10* (17), 9932-9942.
15. Chen, Y. X.; Ye, S.; Heinen, M.; Jusys, Z.; Osawa, M.; Behm, R. J., Application of In-situ Attenuated Total Reflection-Fourier Transform Infrared Spectroscopy for the Understanding of Complex Reaction Mechanism and Kinetics: Formic Acid Oxidation on a Pt Film Electrode at Elevated Temperatures. *J. Phys. Chem. B* **2006,** *110* (19), 9534-9544.
16. Zhang, X.; Choi, I.; Qu, D.; Wang, L.; Lee, C.-W. J., Coverage-dependent electro-catalytic activity of Pt sub-monolayer/Au bi-metallic catalyst toward methanol oxidation. *Int. J. Hydrog. Energy* **2013,** *38* (14), 5665-5670.
17. Park, I.-S.; Chen, D.-J.; Atienza, D. O.; Tong, Y. J., Enhanced CO monolayer electro-oxidation reaction on sulfide-adsorbed Pt nanoparticles: A combined electrochemical and in situ ATR-SEIRAS spectroscopic study. *Catal.Today* **2013,** *202*, 175-182.
18. Grabow, L. C.; Hvolbæk, B.; Nørskov, J. K., Understanding Trends in Catalytic Activity: The Effect of Adsorbate – Adsorbate Interactions for CO Oxidation Over Transition Metals. *Top. Catal.* **2010,** *53* (5), 298-310.
19. Borodziński, A.; Bonarowska, M., Relation between Crystallite Size and Dispersion on Supported Metal Catalysts. *Langmuir* **1997,** *13* (21), 5613-5620.
20. Qiu, X.; Zhang, H.; Dai, Y.; Zhang, F.; Wu, P.; Wu, P.; Tang, Y., Sacrificial Template-Based Synthesis of Unified Hollow Porous Palladium Nanospheres for Formic Acid Electro-Oxidation. *Catalysts* **2015,** *5* (2).
21. Zhang, X.; Yin, H.; Wang, J.; Chang, L.; Gao, Y.; Liu, W.; Tang, Z., Shape-dependent electrocatalytic activity of monodispersed palladium nanocrystals toward formic acid oxidation. *Nanoscale* **2013,** *5* (18), 8392-8397.
22. Kucernak, A. R. J.; Fahy, K. F.; Sundaram, V. N. N., Facile synthesis of palladium phosphide electrocatalysts and their activity for the hydrogen oxidation, hydrogen evolutions, oxygen reduction and formic acid oxidation reactions. *Catal. Today* **2016,** *262*, 48-56.
23. Sathe, B. R.; Balan, B. K.; Pillai, V. K., Enhanced electrocatalytic performance of interconnected Rh nano-chains towards formic acid oxidation. *Energy Environ. Sci.* **2011,** *4* (3), 1029-1036.

24. Xiong, Y.; Dong, J.; Huang, Z.-Q.; Xin, P.; Chen, W.; Wang, Y.; Li, Z.; Jin, Z.; Xing, W.; Zhuang, Z.; Ye, J.; Wei, X.; Cao, R.; Gu, L.; Sun, S.; Zhuang, L.; Chen, X.; Yang, H.; Chen, C.; Peng, Q.; Chang, C.-R.; Wang, D.; Li, Y., Single-atom Rh/N-doped carbon electrocatalyst for formic acid oxidation. *Nat. Nanotechnol.* **2020,** *15* (5), 390-397.
25. Brummer, S. B.; Makrides, A. C., Adsorption and Oxidation of Formic Acid on Smooth Platinum Electrodes in Perchloric Acid Solutions. *J. Phys. Chem.* **1964,** *68* (6), 1448-1459.
26. Chen, W.; Kim, J.; Sun, S.; Chen, S., Electro-oxidation of formic acid catalyzed by FePt nanoparticles. *Phys. Chem. Chem. Phys.* **2006,** *8* (23), 2779-2786.
27. Kapusta, S.; Hackerman, N., The Electroreduction of Carbon Dioxide and Formic Acid on Tin and Indium Electrodes. *J. Electrochem. Soc.* **1983,** *130* (3), 607-613.
28. Chang, S.-C.; Weaver, M. J., Coverage- and potential-dependent binding geometries of carbon monoxide at ordered low-index platinum- and rhodium-aqueous interfaces: comparisons with adsorption in corresponding metal-vacuum environments. *Surf. Sci.* **1990,** *238* (1), 142-162.
29. Park, S.; Xie, Y.; Weaver, M. J., Electrocatalytic Pathways on Carbon-Supported Platinum Nanoparticles: Comparison of Particle-Size-Dependent Rates of Methanol, Formic Acid, and Formaldehyde Electrooxidation. *Langmuir* **2002,** *18* (15), 5792-5798.
30. Weaver, M. J.; Chang, S. C.; Leung, L. W. H.; Jiang, X.; Rubel, M.; Szklarczyk, M.; Zurawski, D.; Wieckowski, A., Evaluation of absolute saturation coverages of carbon monoxide on ordered low-index platinum and rhodium electrodes. *J. Electroanal. Chem.* **1992,** *327* (1), 247-260.
31. Wang, J.-Y.; Zhang, H.-X.; Jiang, K.; Cai, W.-B., From HCOOH to CO at Pd Electrodes: A Surface-Enhanced Infrared Spectroscopy Study. *J. Am. Chem. Soc.* **2011,** *133* (38), 14876-14879.
32. Hahn, F.; Beden, B.; Lamy, C., In situ infrared reflectance spectroscopic study of the adsorption of formic acid at a rhodium electrode. *J. Electroanal. Chem.* **1986,** *204* (1), 315-327.
33. Tang, Y.; Roberts, C. A.; Perkins, R. T.; Wachs, I. E., Revisiting formic acid decomposition on metallic powder catalysts: Exploding the HCOOH decomposition volcano curve. *Surf. Sci.* **2016,** *650*, 103-110.
34. Cuesta, A.; Cabello, G.; Osawa, M.; Gutiérrez, C., Mechanism of the Electrocatalytic Oxidation of Formic Acid on Metals. *ACS Catal.* **2012,** *2* (5), 728-738.
35. Yoo, J. S.; Abild-Pedersen, F.; Nørskov, J. K.; Studt, F., Theoretical Analysis of Transition-Metal Catalysts for Formic Acid Decomposition. *ACS Catal.* **2014,** *4* (4), 1226-1233.
36. McPherson, I. J.; Ash, P. A.; Jones, L.; Varambhia, A.; Jacobs, R. M. J.; Vincent, K. A., Electrochemical CO Oxidation at Platinum on Carbon Studied through Analysis of Anomalous in Situ IR Spectra. *J. phys. Chem. C* **2017,** *121* (32), 17176-17187.
37. Gilman, S., The Mechanism of Electrochemical Oxidation of Carbon Monoxide and Methanol on Platinum. II. The "Reactant-Pair" Mechanism for Electrochemical Oxidation of Carbon Monoxide and Methanol1. *J. Phys. Chem.* **1964,** *68* (1), 70-80.
38. Urchaga, P.; Baranton, S.; Coutanceau, C.; Jerkiewicz, G., Evidence of an Eley–Rideal Mechanism in the Stripping of a Saturation Layer of Chemisorbed CO on Platinum Nanoparticles. *Langmuir* **2012,** *28* (36), 13094-13104.
39. Rodriguez, P.; Garcia-Araez, N.; Koper, M. T. M., Self-promotion mechanism for CO electrooxidation on gold. *Phys. Chem. Chem. Phys.* **2010,** *12* (32), 9373-9380.
40. Gómez-Marín, A. M.; Hernández-Ortiz, J. P., Langmuir–Hinshelwood Mechanism Including Lateral Interactions and Species Diffusion for CO Electro-Oxidation on Metallic Surfaces. *J. Phys. Chem. C* **2014,** *118* (5), 2475-2486.
41. Veser, G.; Esch, F.; Imbihl, R., Regular and irregular spatial patterns in the catalytic reduction of NO with NH3 on Pt(100). *Catal. Lett.* **1992,** *13* (4), 371-382.
42. Zhdanov, V. P., Pattern Formation in Catalytic Reactions Due to Lateral Adsorbate−Adsorbate Interactions. *Langmuir* **2001,** *17* (5), 1793-1799.
43. Barroo, C.; Wang, Z.-J.; Schlögl, R.; Willinger, M.-G., Imaging the dynamics of catalysed surface reactions by in situ scanning electron microscopy. *Nat. Catal.* **2020,** *3* (1), 30-39.
44. Shinagawa, T.; Garcia-Esparza, A. T.; Takanabe, K., Insight on Tafel slopes from a microkinetic analysis of aqueous electrocatalysis for energy conversion. *Sci. Rep.* **2015,** *5* (1), 13801.
45. Fu, W.; Shu, S.; Li, J.; Shi, X.; Lv, X.; Huang, Y.-X.; Dong, F.; Jiang, G., Identifying the rate-determining step of the electrocatalytic hydrodechlorination reaction on palladium nanoparticles. *Nanoscale* **2019,** *11* (34), 15892-15899.
46. Fang, Y.-H.; Liu, Z.-P., Tafel Kinetics of Electrocatalytic Reactions: From Experiment to First-Principles. *ACS Catal.* **2014,** *4* (12), 4364-4376.